AIAA 81-0054R

Effects of Rotation and Blade Incidence on Properties of Turbomachinery Rotor Wake

B. Lakshminarayana,* T. R. Govindan,† and B. Reynolds‡
The Pennsylvania State University, University Park, Pa.

An experimental investigation of the effects of the speed of rotation on a turbomachinery rotor blade wake was conducted using a fan rotor in incompressible flow. Measurements were made at two different rotational speeds (1753 and 1010 rpm) with the same blade incidence angle. The blade incidence angle was also varied to discern the effect of blade loading. A three-sensor hot-wire probe mounted in a stationary frame of reference was used for the measurements made at several radial and axial stations in the near- and far-wake regions. The three-dimensional mean velocity and turbulence profiles, the wake defect, wake decay rate, turbulence intensities, and turbulence stresses are appreciably altered when the speed of rotation and the blade loading are changed. The wake defect is reduced and the radial velocity increased when the rotation speed is increased.

Nomenclature

C = chord length
i = incidence
L_P, L_S = wake width at half the depth on the pressure and suction sides of the wake, respectively
N = speed, rpm
p = static pressure
P.S. = pressure side
Q = resultant velocity in the relative (rotating) frame of reference
r_m = mean radius
R = radius ratio (r/r_t)
r, θ, z = radial, tangential, and axial coordinates, respectively ($z = 0$ at trailing edge)
S = blade spacing
S.S. = suction side
s, n, r = streamwise, normal, and radial coordinates ($s = 0$ at trailing edge, $n = 0$ at the wake center)
U, V, W = radial, tangential, and axial velocities (mean) in rotating coordinate system (U is positive in radial outward direction)
U_n, U_r, U_s = relative mean velocities in the normal, radial, and streamwise directions, respectively
u_n', u_r', u_s' = fluctuating components of relative velocities in the normal, radial, and streamwise directions, respectively
u', v', w' = fluctuating component of radial, tangential, and axial velocities
v, w = defect in relative tangential and axial mean velocities
$(V_\theta)_{abs}$ = absolute tangential velocity
Y = tangential distance from the wake centerline nondimensionalized by semiblade spacing ($2r\theta/S$, $\theta = 0$ at wake centerline, and Y is negative on the suction side and positive on the pressure side of the wake)
Z = axial distance from rotor blade trailing edge, nondimensionalized by chord length of rotor blade
λ = stagger angle
δ = wake width $2(L_P + L_S)/S$
Ω = angular velocity of the rotor
ψ = mass averaged pressure rise coefficient
ρ = density
ϕ = flow coefficient ($W_1/\Omega r_m$)
β = flow angle measured from the axial direction
θ_c = camber angle
$\tau_r, \tau_z, \tau_\theta$ = normalized turbulence intensities in the radial, axial, and tangential directions, respectively ($\sqrt{\overline{u'^2}}/W_0$, $\sqrt{\overline{w'^2}}/W_0$, $\sqrt{\overline{v'^2}}/W_0$)
τ_{sn}, τ_{rn} = streamwise and radial stresses, respectively ($-\overline{u_s' u_n'}/Q_0^2$, $-\overline{u_r' u_n'}/Q_0^2$)

Subscripts

c = at the wake centerline
m = maximum value in wake
t = at the tip
0 = freestream/wake edge value
$1,2$ = inlet and outlet of rotor, respectively
abs = absolute
P,S = pressure and suction sides, respectively

Introduction

ROTOR wakes, which represent the flowfield downstream of the rotor, are not only influenced by upstream flowfield conditions but are also controlled by such parameters as blade spacing, solidity, hup-tip ratio, blade loading, distance from the blade trailing edge, and centrifugal and Coriolis forces induced by curvature and rotation. These effects make the flow highly three-dimensional, which introduces many complications in experimental and theoretical investigations of the rotor wake.

Lack of knowledge of the flowfield downstream of a compressor rotor blade has hampered progress in compressor design, development and prediction of losses, noise generation, surge and stall, and three-dimensional flow into the subsequent blade row. All the earlier investigations (e.g., Refs. 1 and 2) were confined to a study of a rotor wake at one operating condition (blade loading, geometry, speed, etc.). A review of the earlier investigation on rotor wake is given in Ref. 3. There has not yet been an investigation on the effects of rotation on the wake properties in a subsonic rotor.

The present study is directed toward an understanding of the effects of rotation and blade loading on the rotor wake structure. It is known that the rotation induced centrifugal and Coriolis forces generate spanwise flows inside the blade boundary layers, the magnitude of which depends on the angular velocity of the rotor and the blade loading. These

Presented as Paper 81-0054 at the AIAA 19th Aerospace Sciences Meeting, St. Louis, Mo., Jan. 12-15, 1981; submitted Feb. 19, 1981; revision received July 27, 1981.

*Director of Computational Fluid Dynamics Studies and Professor of Aerospace Engineering, Dept. of Aerospace Engineering. Associate Fellow AIAA.

†Graduate Assistant, Dept. of Aerospace Engineering.

‡Graduate Assistant, Dept. of Aerospace Engineering (presently, Development Engineer, Avco Lycoming Division, Stratford, Conn.).

spanwise flows result in a decrease of the blade boundary-layer thickness (or wake width) near the hub and an increase near the tip.

Both the Reynolds number and the rotation effects are present in the data given in the paper. It is difficult to separate these effects in turbomachinery. Even though the authors feel that the Reynolds number effects should be small in the range of Reynolds number employed in this paper, some caution should be exercised in interpreting the data for the effects of rotation.

This investigation was carried out using a fan rotor. The blades had incidence and camber, and differed from the ones used earlier in Refs. 1 and 2. The blades had high loading. The investigation included a study of the wake velocity and the turbulence profiles and their decay characteristics at three different rotational speeds and at two different loadings. A three-sensor hot wire and an ensemble averaging technique were employed in this investigation.

Facility and Measurement Technique

Measurements reported in this paper were carried out using the Axial Flow Fan Research Facility (AFRF) at the Applied Research Laboratory. The facility and the rotor are described in detail in Ref. 4. A brief description follows.

Rotor Characteristics

A nine-bladed rotor with cambered blades was installed in the facility and had the following specifications: tip diameter = 0.54 m, hub/tip diameter ratio = 0.44, blade chord (const) = 15.24 cm, maximum thickness (const) = 1.5 cm. Other relevant data are tabulated in Table 1.

The performance characteristic of the rotor is shown in Fig. 1. The rotor alone (no IGV or stator) was operated at the design point shown in Fig. 1 at two different rotational speeds, $N = 1753$ and 1010 rpm. Identical inlet incidence ($i = 3$ deg at midradius) at two differing rotational speeds was achieved by means of an auxiliary fan at the exit of the facility. Thus the effects of rotation on the rotor wake were isolated from the effects of the blade loading by maintaining the same incidence at two different rotational speeds. The axial velocities at the design conditions were 21 and 12 ms at 1753 and 1010 rpm, respectively. The Reynolds number based on the inlet relative velocity and chord length at the midspan were 4.2×10^5 and 2.4×10^5 at 1753 and 1010 rpm, respectively. An additional measurement was made at the off design condition at a flow coefficient of 0.7 ($i = -1$ deg at midradius) as shown in Fig. 1. This test was run at 1499 rpm. These sets of measurements provide the wake data at two differing speeds (1753 and 1010 rpm) at the same blade loading ($\phi = 0.6$) and two different blade loadings ($\phi = 0.6$ and 0.7). The measurements were taken at the following axial and radial stations at these operating conditions:

$R = 0.453, 0.488, 0.511, 0.534, 0.628, 0.72, 0.813,$
$0.91, 0.93, 0.953$

$Z = 0.042, 0.084, 0.125, 0.167, 0.208, 0.25, 0.29,$
$0.333, 0.664, 1.331$

These measurements provide data both in the near- and far-wake regions.

Table 1 Rotor blade characteristics (design)

R	C/S	λ, deg	θ_c, deg	β_1, deg	β_2, deg	i, deg
0.44	1.81	23.14	35.64	45.66	13.21	4.70
0.50	1.61	31.02	28.12	49.06	24.35	3.98
0.61	1.31	42.44	17.87	54.68	40.01	3.30
0.72	1.11	50.28	11.74	57.08	47.87	2.94
0.83	0.96	55.78	8.01	63.59	58.48	2.80
0.94	0.85	59.85	5.71	65.43	61.18	2.72
1.0	0.80	61.59	4.80	66.65	63.06	2.66

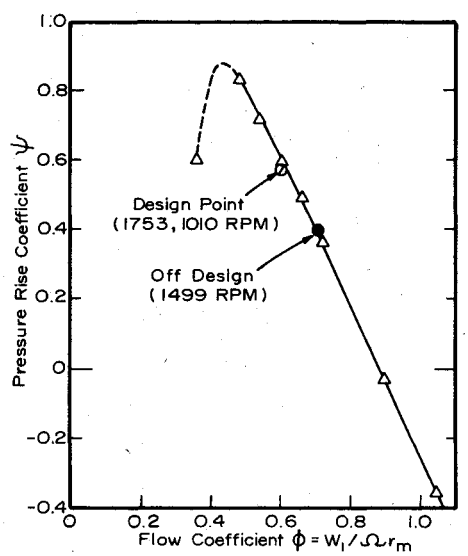

Fig. 1 Performance characteristics of AFRF nine-bladed fan rotor.

Measurement Program

The measurements were carried out in a stationary reference frame using a miniature three-sensor hot-wire probe located downstream of the trailing edge. The four major steps in data processing were: analog to digital conversion, translation for IBM 370, determination of every tenth wake, and ensemble averaging of digital data. This technique is described in Refs. 3 and 5. Approximately 366 digital points were used to derive the blade-to-blade variation in measured quantities. The one spike per revolution signal peak was used as an accurate measure of one rotor revolution in any time base. The probe and the technique are described in Ref. 3.

Mean Velocity Profiles

The hot-wire data outside the hub and annulus wall regions at $R = 0.628$, 0.72, and 0.813 and at various axial locations are presented in this paper. The data include the effects of rotation as well as blade loading. The data, unless otherwise stated, are in the relative frame of reference in axial z, tangential θ, and radial coordinate r system. The tangential distance Y is normalized by the semiblade spacing. Hence $Y = 0$ represents the wake center, $Y = \pm 1.0$ represents the midpassage. All velocities are normalized by the corresponding freestream axial velocity, the intensities by the square of the freestream axial velocity, and the stresses by the square of the freestream resultant velocity. The profiles at $R = 0.628$ and 0.813 consist of only the near-wake data at $Z = 0.042$, 0.084, 0.125, and 0.167, while the profiles at $R = 0.72$ include both the near- and far-wake data at $Z = 0.042$, 0.084, 0.664, and 1.331. Since the data set includes more than 366 points in one blade passage, the profiles are shown as continuous curves rather than discrete points.

Since all the data presented in this paper are nondimensionalized by W_0, their values at $Z = 0.166$ are shown in Table 2. Variation of this quantity downstream is found to be negligible.

Table 2 Freestream axial velocity (W_0) at $Z = 0.166$

R	0.534	0.628	0.72	0.813
W_0, ms 1753 rpm	23.3	19.7	25.5	22.1
W_0, ms 1010 rpm	17.3	13.7	16.3	14.2

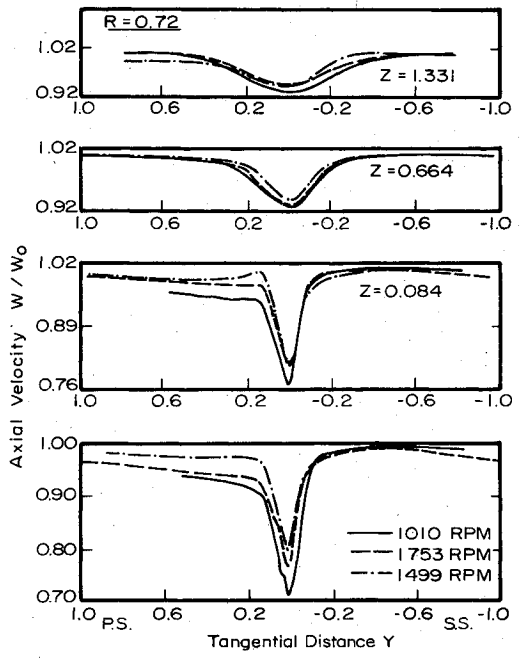

Fig. 2 Axial velocity profile at $R=0.72$, $\phi=0.6$ (1010 and 1753 rpm) and 0.7 (1499 rpm) (see Table 2 for value of W_0).

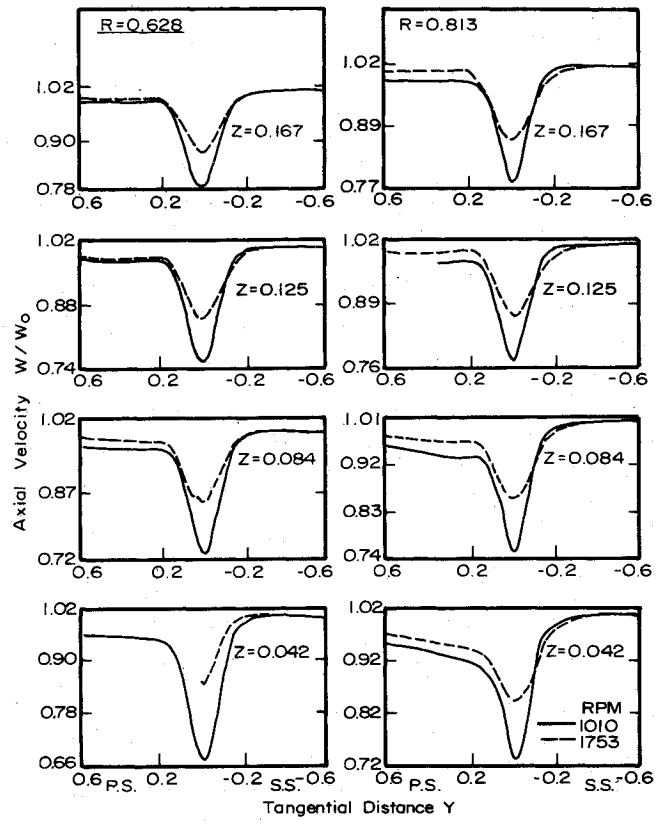

Fig. 3 Axial velocity profile at $R=0.628$ and 0.813, $\phi=0.6$ (see Table 2 for values of W_0).

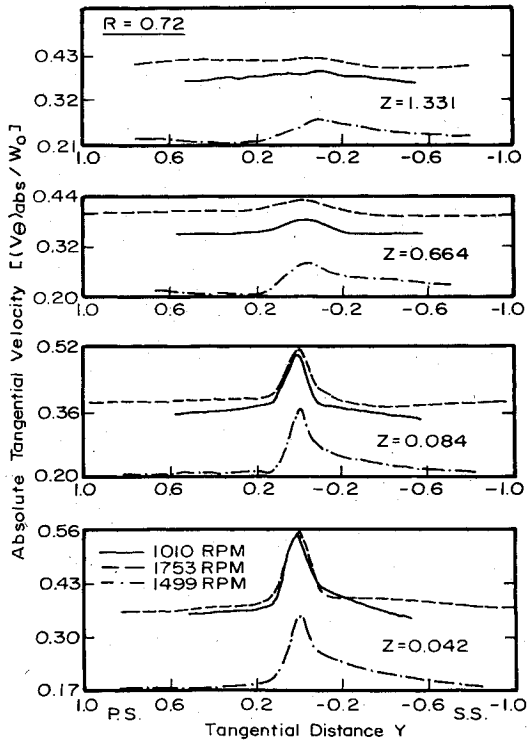

Fig. 4 Absolute tangential velocity profile $R=0.72$, $\phi=0.6$ (1010 and 1753 rpm) and 0.7 (1499 rpm).

It is evident from the investigations reported in Ref. 6 that the Reynolds number effect is small in the Reynolds number range of $2.5\text{-}5\times10^5$. Less than 0.5% change in efficiency, 3% change in pressure rise coefficient, and negligible change in outlet angle were observed in this range. The effect of rotation is felt in the magnitude of the radial velocities in the blade boundary layer, the hub-to-tip variation of the blade boundary-layer growth, wake defect, and the turbulence characteristics in the wake. This in turn affects the wake decay downstream of the rotor. The turbulence intensity components as well as Reynolds stresses are affected by rotation as explained in Ref. 7. This will affect the boundary-layer growth as well as the decay of the wake and its variation in the radial direction. Hence the effect of the increase in speed is twofold: it increases the Coriolis force and alters the turbulence intensities and stresses. It increases the three-dimensionality of the wake by increasing the radial velocities. These effects tend to decay the wake more rapidly, at least in the near-wake region where the history effects persist.

Axial Velocity Profiles

The axial velocity profiles near the midradius are shown in Fig. 2. The defect is nearly 30% for the lowest speed at $Z=0.042$. This indicates rapid decay of the rotor wake. The axial velocity defect decreases with the increase in speed (at constant loading) and decrease in the blade loading. This trend persists even up to half-a-chord downstream, beyond which there are no noticeable differences in profiles for various operating conditions. The asymmetry in the wake and the inviscid effects persist even up to $Z=0.084$, beyond which the effects of loading and the speed vanish, providing not only identical but also symmetrical axial velocity profiles in the wake. It is clear that higher speeds result in lower axial velocity defect and higher loading increases the velocity defect (or decreases the decay rate of the velocity defect). Similar conclusions have been drawn by Gallus et al.[8] on the basis of tests carried out in a high-speed rotor without IGV. The wake width at a fixed loading does not change with increase in the speed.

The axial velocity profiles at radii below ($R=0.628$) and above ($R=0.813$) midspan are shown in Fig. 3 for the same loading at two different speeds. The effect of change in the rotational speed is much more evident in these regions. The defect in the axial velocity near the trailing edge decreases as much as 35% when the speed is increased from 1010 to 1753 rpm. This trend persists at both radii and even at $Z=0.167$. The wake width is nearly the same at both speeds. Since the loading of the blades was the same the wake width is the same for the two rotational speeds. This is expected as the growth

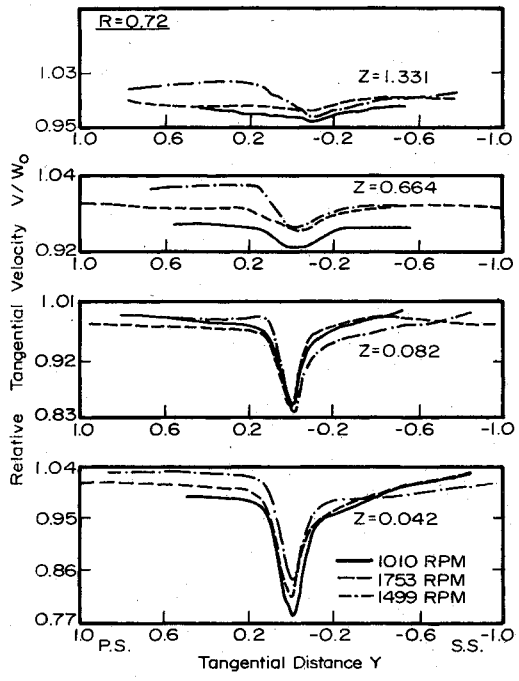

Fig. 5 Relative tangential velocity profile $R=0.72$, $\phi=0.6$ (1010 and 1753 rpm) and 0.7 (1499 rpm).

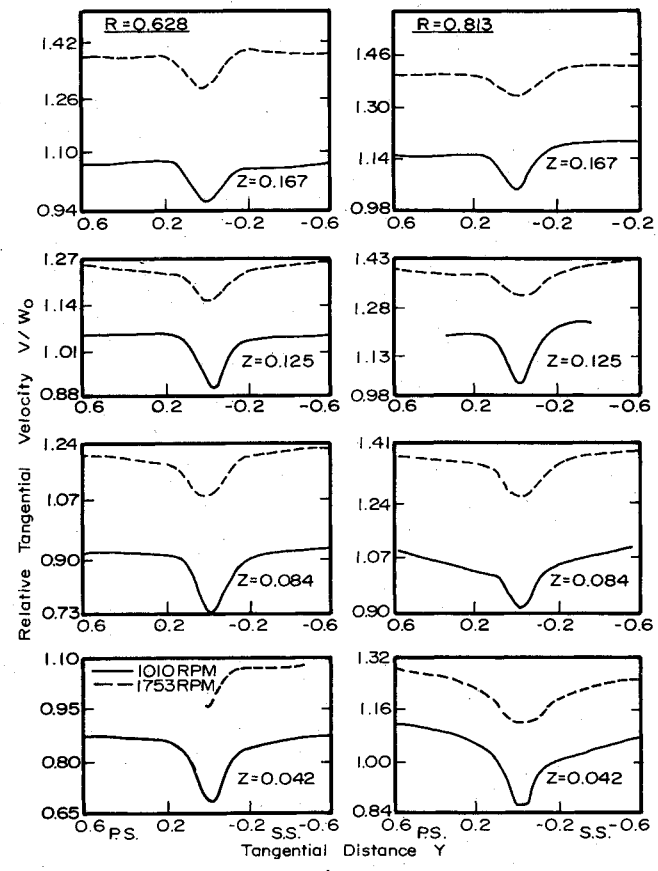

Fig. 6 Relative tangential velocity profile $R=0.628$ and 0.813, $\phi=0.6$.

of the boundary layer is primarily a function of the blade loading. But higher rotational speeds induce higher radial velocities and turbulence intensities inside the blade boundary layer and the wake and, as explained earlier, are responsible for more rapid mixing of the wake. Since the wake width is nearly constant, the absolute tangential velocities are nearly identical at both speeds (see Fig. 4), the rapid decay of the wake near the trailing edge is evidently due to rotation.

Tangential Velocity Profiles

The absolute tangential velocity $(V_\theta)_{abs}$ profile at midradius at two different blade loadings ($\phi=0.6$ and 0.7) and at two different speeds at the same loading ($\phi=0.6$) is shown in Fig. 4. The absolute tangential velocities are lower, as expected at $\phi=0.7$, but the differences between the two speeds at $\phi=0.6$ are negligible for $Z\leq 0.084$. Far downstream ($Z\geq 0.664$), the tangential velocities are generally higher at higher speeds. This is probably caused by the transport of higher angular momentum fluid near the hub toward the midradius at higher speeds.

The relative tangential velocity profiles at $R=0.72$ are shown in Fig. 5. The data at lower loading ($\phi=0.7$) show the least defect near the trailing edge ($Z=0.042$) and the profiles are almost identical at $Z=0.082$ for all operating conditions. The effect of speed is also evident from this plot. The data at higher speeds show smaller velocity defect and faster decay of the wake at all axial stations.

The relative tangential velocities at $R=0.628$ and 0.813 and at $\phi=0.6$ for two different speeds are shown in Fig. 6. The effect of speed is much more dominant at these radii. Faster decay of the wake defect at higher speeds is clearly evident from these plots.

Radial Velocity Profiles

Radial velocities are caused by an imbalance in the radial pressure gradients and the centrifugal forces. Physically at either surface of the trailing edge of a compressor rotor blade, the radial velocities must be zero while the maximum radial outward velocities occur slightly away from the blade surface. A trailing vortex system associated with the circulation might give a radially inward flow on one side and radially outward flow on the other side of the blade.

The radial velocity profiles at midradius for $\phi=0.6$ (1010 and 1753 rpm) and $\phi=0.7$ (1499 rpm) are shown plotted in Fig. 7. Near the wake center as well as in the freestream nearly zero radial velocity and radially inward flow near the pressure surface and radially outward flow near the suction side exist for $\phi=0.6$ at both speeds. This situation is possible if the trailing vortex dominates the flow in the trailing-edge region while the boundary-layer flow dominates the flow in the near- and far-wake regions. This complex flow phenomenon is not fully understood and a knowledge of the flow on the blades (blade boundary layer) could assist in explaining its nature. The profile at $N=1499$ rpm, $\phi=0.7$ shows a trend opposite to that at $\phi=0.6$. The radial inward flow occurs near the suction side and outward flow near the pressure side. The peak radial velocities are higher at low speed, a result contradictory to earlier hypothesis. But these radial velocity profiles undergo a rapid change as they travel downstream. At $Z=0.084$, the radial velocity at $\phi=0.7$ remains almost the same as that at $Z=0.042$, while that for $\phi=0.6$, $N=1010$ rpm have decreased substantially. The radial velocity is mostly inward for the lower speed (1010 rpm) at $Z=0.084$.

The radial velocity profiles at $R=0.628$ and 0.813 at the same loading ($\phi=0.6$) and at two different speeds are shown in Fig. 8. The radial velocities are higher at higher speeds at all the radial and the axial ($Z=0.042$ to 0.167) locations. At $R=0.628$, the radial velocities are always outward, with smaller velocity at the wake center. One possible reason for the large radial velocity in this region may be the presence of large design flow turning and stagger angle changes in the region $R=0.44$ to 0.61 (see Table 1), beyond which the change is more gradual. The radial velocity seems to decay from $Z=0.042$ to 0.082, beyond which ($0.167>Z>0.084$) the radial velocities increase with generally higher magnitude near the suction side. This may have been caused by the presence of the hub wall and the growth of the secondary vortex in this region. The radial velocities at 1753 rpm are almost twice as much as those at 1010 rpm.

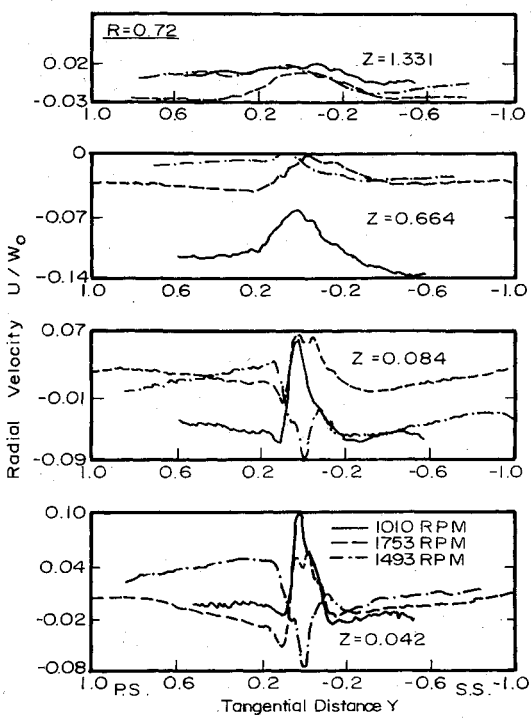

Fig. 7 Radial velocity profile $R=0.72$, $\phi=0.6$ (1010 and 1753 rpm) and 0.7 (1499 rpm).

The radial velocities at $R=0.813$ are lower than those at $R=0.628$ and are of the same order of magnitude as those observed at the midradius. Here again, the radial velocities are higher at higher speeds and the decay of the radial velocity in the trailing-edge region is slower than the axial and tangential components. The radial velocities are found to be substantial even in the freestream at both radii for the 1753 rpm case. This indicates the increase in three-dimensional effects when the speed is increased.

Decay of Wake Properties

The decay of the axial velocity defect, maximum radial velocity $[(U_P - U_S)_m]$ and the tangential velocity defect, all normalized by the freestream axial velocity are plotted in Fig. 9 for $R=0.72$. Data at all the operating conditions are shown. As explained earlier, it is clear that the defects are maximum at the lower speed and minimum at the lowest loading tested. But the wake defect at lower speeds decays more rapidly to provide nearly identical values far downstream ($Z=1.331$). Near the trailing edge, the radial velocities are maximum at the lower speed and minimum at lower loading. The radial velocities decay rapidly to reach very small values far downstream. The tangential velocity defect decays much more rapidly than the axial velocity defect. The contributing factor to the very rapid decay of the tangential velocities is the radial component of velocity as well as the radial distribution of freestream tangential and axial velocities.

Radial Variation of Wake Properties

The radial variation of the axial velocity defect and the tangential velocity at the wake center, and the maximum difference in radial velocity $(U_P - U_S)_m$ are shown in Fig. 10 for $Z=0.042$ and 0.167 at 1010 and 1753 rpm.

It is evident that the axial velocity defect at the wake center is maximum at all the radii for $Z=0.042$ at 1010 rpm, with the highest value near the hub and lowest value near the tip. This may partially be due to the fact that at any downstream axial station, the wake at outer radii will have travelled a larger distance than the wake near the hub due to the increased outlet angle near the tip. The defect in axial velocity decreases rapidly downstream.

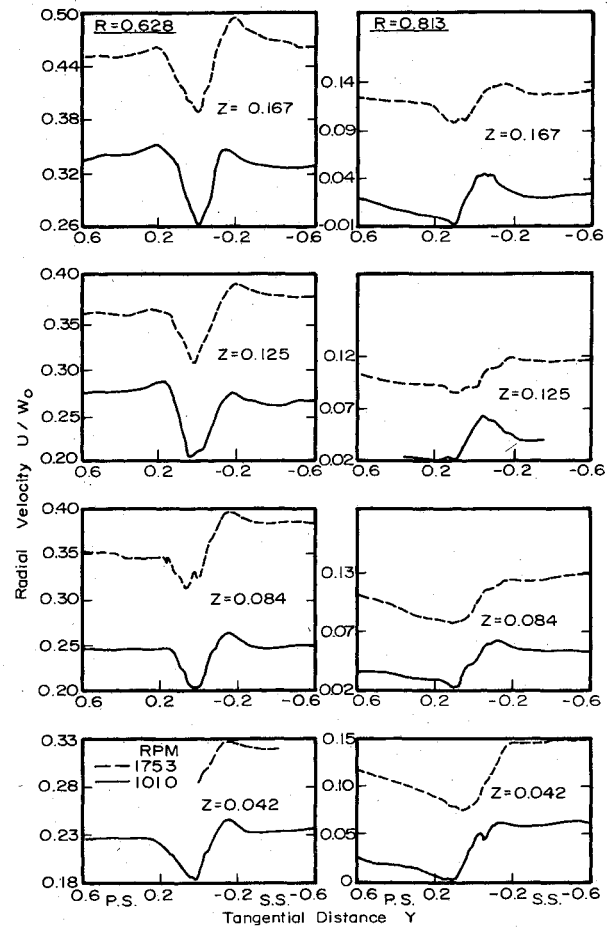

Fig. 8 Radial velocity profile $R=0.628$ and 0.813, $\phi=0.6$.

The radial variation of the relative tangential velocity at the wake center is also plotted in Fig. 10. The actual velocity rather than the defect is plotted in view of the radial variation of the design values of V_0 from hub to tip. It is evident that the velocity is minimum (or the defect is maximum) for the low-speed case, with lowest velocity occurring near the hub.

The difference in radial velocity $[(U_P - U_S)_m]$ generally decreases from the hub to the tip, with appreciable reduction near the tip. This indicates the influence of annulus wall in reducing the radial velocities.

Wake Width

The downstream variation of the wake width at $R=0.72$ for various operating conditions is shown plotted in Fig. 11. For $\phi=0.6$, the initial wake widths differ by a small amount at two different speeds, but reach nearly the same value far downstream. The width is lower at the lower loading and the growth is also less rapid.

The radial variation of the wake width at $Z=0.042$ and 0.167 at 1753 and 1010 rpm is also shown in Fig. 11. The wake width is higher at the hub at 1010 rpm, but remains the same at $R=0.621$ and 0.72 for both speeds. But near the tip, the trend is reversed, the higher speed case has a larger width than the 1010 rpm case. The reasons for this behavior are obvious. As the speed is increased (at the same loading), the radial velocity increases and hence there is a larger migration of boundary layer and wake flow away from the hub and toward the tip. This is clear from Fig. 11. Another interesting feature is that the wake width changes little from $Z=0.042$ to 0.167 near midradius, while the width increases substantially near the hub.

Turbulence Properties

A qualitative analysis of the effects of rotation on the turbulence structure of rotor wakes has been developed by

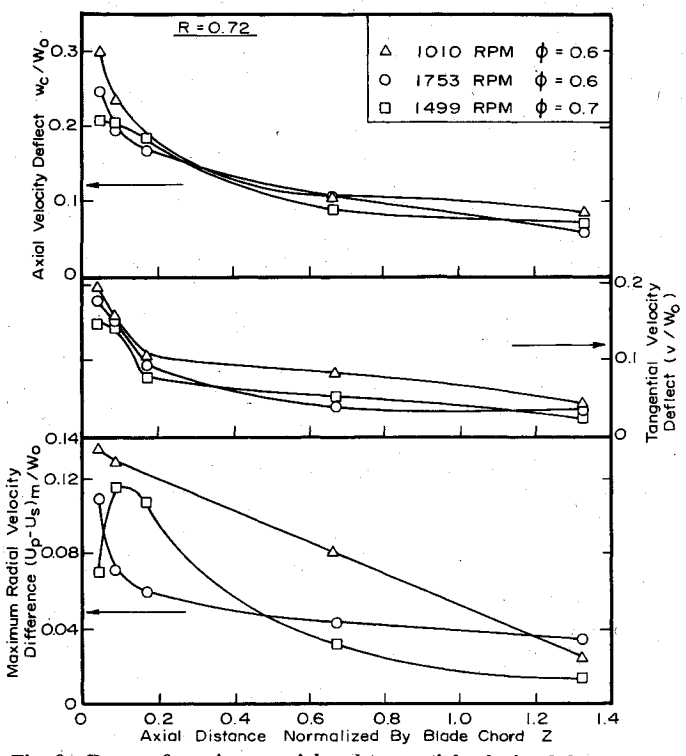

Fig. 9 Decay of maximum axial and tangential velocity defects and the radial velocity.

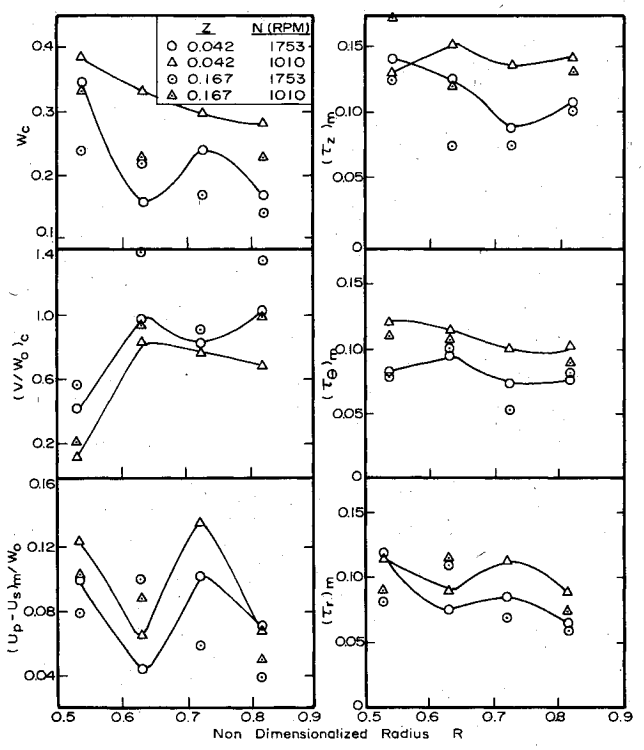

Fig. 10 Radial variation of wake properties for $\phi = 0.6$.

Lakshminarayana and Reynolds.[7] One of the important conclusions of the analysis was that the rotation influences the turbulence structure of the rotor wakes substantially by redistributing its components. Furthermore, they concluded that this redistribution results in an increase in the radial component of the turbulence intensity and shear stress with a corresponding decrease in the streamwise component (the resultant of the axial and tangential components). Similar analyses can be made for the shear stresses. Lakshminarayana and Reynolds[7] concluded that an increase in rotation would

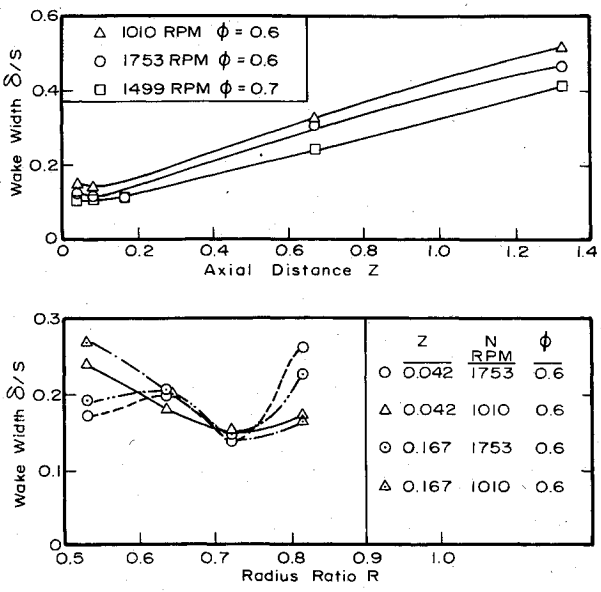

Fig. 11 Axial and radial variation of the wake width.

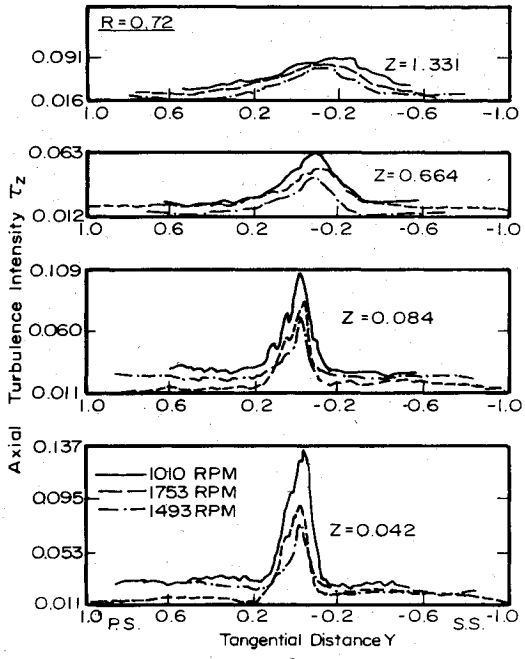

Fig. 12 Axial turbulence intensity profile $R = 0.72$, $\phi = 0.6$ (1010 and 1753 rpm) and 0.7 (1499 rpm).

increase the radial stress while decreasing the streamwise stress. The turbulence data at midradius is presented in this paper. The data at $R = 0.628$ and 0.813 are given in the original version of this paper.[9]

Turbulence Intensity Profiles

All the turbulence intensities presented in this paper are normalized by the freestream axial velocity. The axial-turbulence intensity profiles at $R = 0.72$ are shown in Fig. 12. In the near wake, at $\phi = 0.6$, the profiles at lower speed (1010 rpm) have the highest intensity (13.4%) both in the wake and in the freestream. The effect of rotation vanishes beyond $Z = 0.664$. The effect of the blade loading is also clear from Fig. 12. The maximum intensity at $\phi = 0.7$ is about half the value at $\phi = 0.6$, and $N = 1010$ rpm. There are then two compensating trends when both the rotation and loading are increased, the former decreases the intensity while the latter increases it.

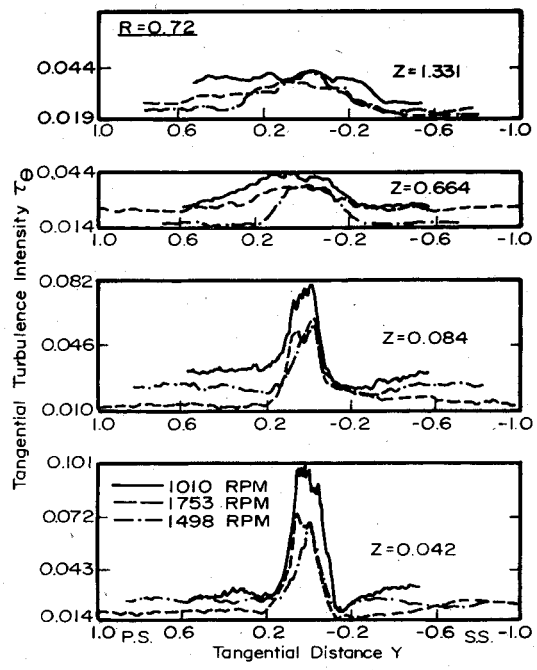

Fig. 13 Tangential turbulence intensity profile $R=0.72$, $\phi=0.6$ (1010 and 1753 rpm) and 0.7 (1499 rpm).

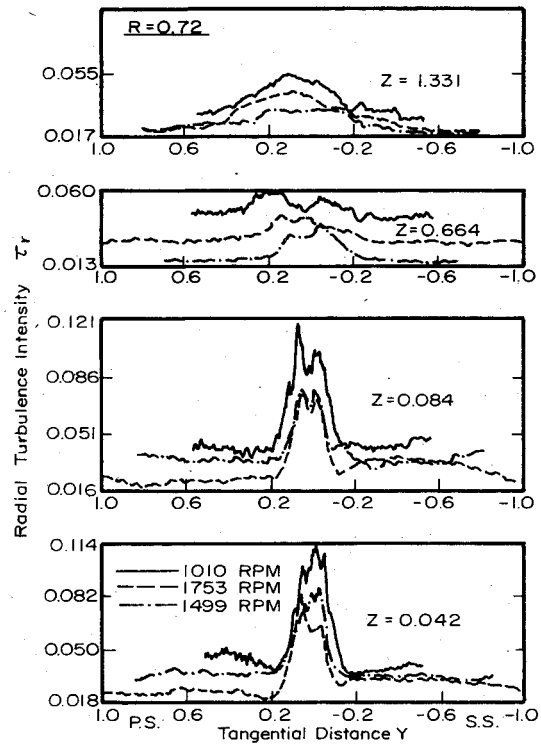

Fig. 14 Radial turbulence intensity profile $R=0.72$, $\phi=0.6$ (1010 and 1753 rpm) and 0.7 (1499 rpm).

The tangential intensity profiles at $R=0.72$ are shown in Fig. 13. These profiles show trends similar to those of the axial intensity profiles. The magnitudes of these intensities are generally lower than the axial component. The peak intensity at $Z=0.042$ is about 10% at 1010 rpm and about 7% at 1753 rpm.

It is expected[7] that the rotation would have a major effect on the radial component of the turbulence intensity. Radial turbulence intensity profiles at $R=0.72$ are shown in Fig. 14. An interesting feature in these plots is that the magnitude of the radial intensity is of the same order of magnitude as the

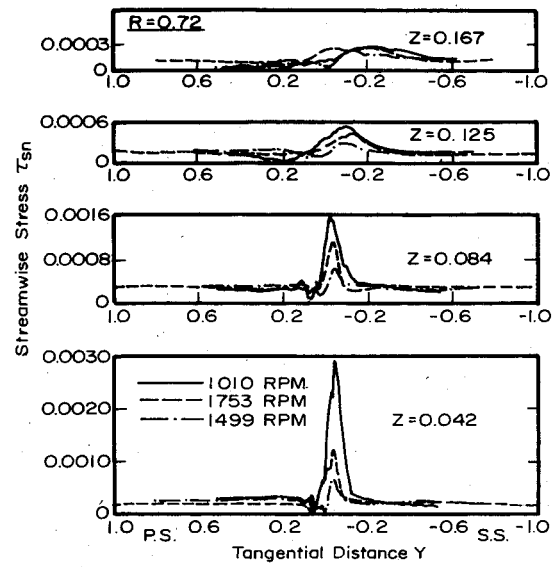

Fig. 15 Streamwise turbulence stress profile $R=0.72$, $\phi=0.6$ (1010 and 1753 rpm) and 0.7 (1499 rpm).

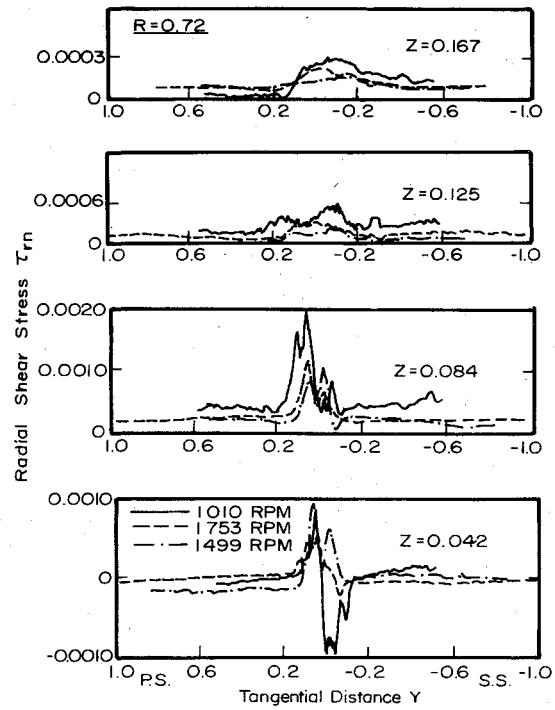

Fig. 16 Radial turbulence stress profile $R=0.72$, $\phi=0.6$ (1010 and 1753 rpm) and 0.7 (1499 rpm).

axial and tangential intensities. In a stationary flow the radial intensities are usually very small and the amplification of this component is one of the major effects of rotation. The effect of loading on these profiles is as would be expected, with lower intensities at the lower loading ($\phi=0.7$). However, contrary to the trend expected, the radial intensities at 1010 rpm are the highest and substantially higher than those at 1753 rpm. The decrease in the radial intensity at 1753 rpm from that at 1010 rpm could have been caused by the decreased production due to the decreased values of the correlations $\overline{u_s' u_n'}$ and $\overline{u_n' u_r'}$ (as concluded later). In such a situation [Ref. 7, Eq. (9)] the radial intensities would be lower at the higher rpm. The earlier statement that rotation amplifies the radial intensity is true only when the effect of the Coriolis force is taken into consideration without any change in the production due to mean velocity gradients.[7]

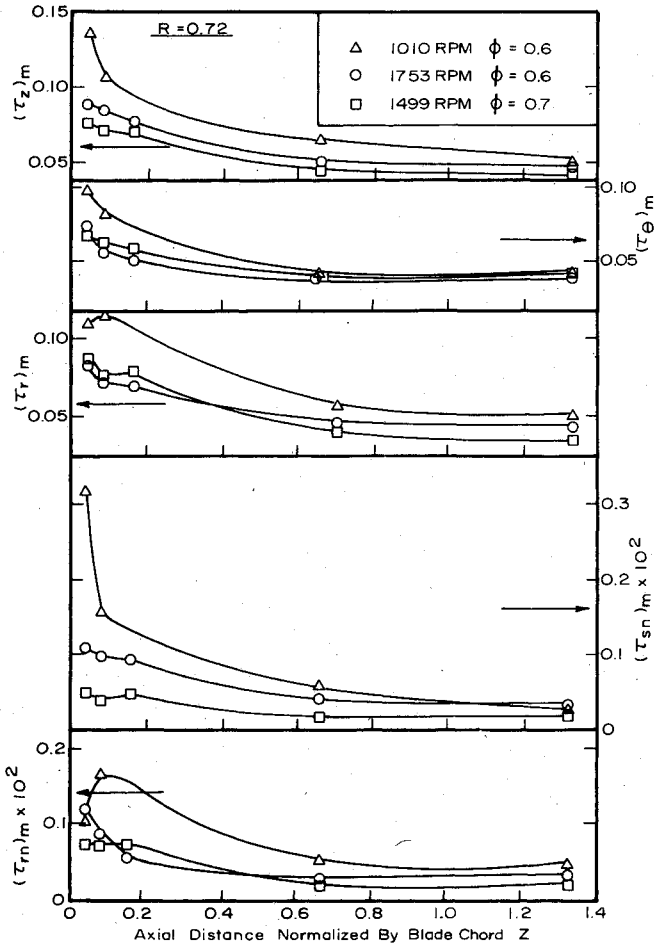

Fig. 17 Decay of maximum axial, tangential, and radial turbulence intensities ($R = 0.72$).

Turbulent Shear Stress Profiles

The turbulent shear stresses of practical interest are the streamwise stress $-\rho\overline{u_s'u_n'}$ and radial stress $-\rho\overline{u_r'u_n'}$. These stresses were derived from the hot-wire data and normalized by the dynamic pressure ρQ_0^2, where Q_0 is the resultant relative velocity in the freestream.

The streamwise shear stress profiles at $R = 0.72$ are shown in Fig. 15. These stresses are lowest at the lower loading (1499 rpm) and highest at the higher loading and lower rpm (1010 rpm). The decay of this stress is more rapid than those of the turbulent intensities, becoming negligibly small for $Z > 0.084$. It is interesting to note that the stress is largest at the lower speed, the loading being the same. This can be explained on the basis of analysis in Ref. 7. The production of the streamwise stress is due to the normal gradient of the streamwise velocity $\overline{u_n'^2}(\partial U_s/\partial n)$ and the Coriolis force $(\overline{u_s'u_n'}2\Omega\cos\beta)$, both of which are affected by the blade loading and the speed of the rotor. The mean velocity data indicate that the mean velocity gradients are smaller at the higher rotational speed. Further, if $(\overline{u_s'u_n'})$ and $(\overline{u_s'u_r'})$ have the same sign (as has been observed in Ref. 10) and the radial stress $(-\rho\overline{u_n'u_r'})$ has a negative value on the suction side and a positive value on the pressure side (as has been observed in results shown in Fig. 16) it can be concluded on the basis of Eq. (10) in Ref. 7 that an increase in rotation should decrease the streamwise stress on the suction side. The same is true on the pressure side. Since the streamwise stresses are reduced by rotation, only small negative values are observed on the pressure side.

The radial component of the turbulent stresses at $R = 0.72$ is shown in Fig. 16. Consistent with the radial velocity profiles (Fig. 7) where both inward and outward velocities are observed on either side of the wake center, the radial stresses are positive on the pressure side and negative on the suction side at $Z = 0.042$. The negative values disappear at $Z = 0.084$ and all stresses reach very low values further downstream. The stresses are highest at 1010 rpm and lowest for the lower blade loading (1499 rpm).

An interesting observation is that even though the radial velocities are much smaller than the streamwise velocity (compare Fig. 7 with Figs. 2 and 5), the radial stresses are about the same order of magnitude as the streamwise stresses. Reasons for this trend have been analyzed by Lakshminarayana and Reynolds.[7] The rotation terms in these equations tend to increase the radial stress and decrease the streamwise stress, producing the observed effect.

At lower blade loading (1499 rpm), the stresses are lowest. This can be explained on the basis of Eq. (11) in Ref. 7, where a decrease in the normal gradient of the radial velocity (as observed in Fig. 7) decreases the production term.

Axial and Radial Variation of Turbulence Properties

The decay of maximum turbulence intensities and stresses at $R = 0.72$ at all operating conditions are shown in Fig. 17. As discussed earlier, the maximum turbulence intensities are highest at lower speed and decrease when the loading is decreased. This effect disappears in the far wake and correspondingly a higher decay rate is observed at lower speed. Furthermore, the effect of rotation in redistributing turbulence energy is clear in Fig. 17 where $(\tau_z)_m > (\tau_r)_m > (\tau_\theta)_m$. In a nonrotating case $(\tau_r)_m$ would be minimum. The intensities decay rapidly and reach nearly constant values in the far wake beyond a half-chord.

The decay of the maximum stresses is also shown in Fig. 17. The trends are similar to that of intensities. The maximum stress increases with loading and decreases with an increase in speed at the same loading. The decay is rapid in the near wake and the stresses are negligible at one chord length downstream. The maximum streamwise shear stress at $Z = 0.042$ and 1010 rpm is nearly three times higher than that at 1753 rpm at the same axial station. The loading and rotation effects on radial and streamwise stresses, seen near the trailing edge, vanish rapidly and disappear beyond $Z = 0.669$. The values of the streamwise and radial stresses are of the same order except at $Z = 0.042$ and 1010 rpm. This clearly reveals the effect of rotation as discussed earlier.

The radial variation of the maximum turbulence intensities is shown in Fig. 10. Both the axial and radial components are higher at the lower rpm and reach maximum values near the hub. The radial turbulence intensities at $Z = 0.042$ are higher at lower rpm, except at $R = 0.52$, and they assume nearly identical values at $Z = 0.167$. The radial turbulence intensities decrease toward the tip, which is consistent with the radial velocity plot shown in Fig. 10.

Conclusions

1) Rotation and blade loading have an appreciable effect on the mean velocity and turbulence profiles. These effects are confined to the near wake region and disappear beyond about a half-chord downstream of the trailing edge.

2) Axial and tangential velocity defects decrease with increase in speed at the same loading and decrease with decrease in loading.

3) Radial velocities increase with both rotation and loading and decay slower than the axial and tangential velocity defects.

4) The absolute tangential velocity is independent of speed in the trailing-edge region. Further downstream the absolute tangential velocity is higher at higher rotation speeds, a consequence of the transport of angular momentum by the radial flow.

5) A major effect of rotation is in the redistribution of the turbulence energy resulting in an amplification of the radial intensities to values of the same order of magnitude as the axial and tangential intensities.

6) At the same blade loading, lower rotation speeds produce higher turbulence intensities and stresses. A decrease in loading decreases all the turbulence intensities and stresses.

7) The decay rate of the mean velocity defects, turbulence intensities, and shear stresses increase for lower speeds and higher loading.

8) The wake width is nearly the same at mid radius at both speeds for the same loading, but is substantially different at the hub and the tip. At the hub, the wake width is higher at the lower speeds. At the tip, it is higher at the higher speeds. This is an indication of the radial migration of fluid toward the tip at higher speeds.

9) At lower loadings the wake width is smaller indicating smaller boundary-layer growth on the blade.

10) The Reynolds number effect is present in all the data presented in this paper. Further efforts should be directed in a study of rotation effect only, keeping all other parameters constant.

Acknowledgments

This work was supported by the National Aeronautics and Space Administration, through Grant NSG 3012, with L. Shaw as the technical monitor. The experimental work was carried out at the Applied Research Laboratory in their Axial Flow Research Fan Facility. Assistance by J. Rishell and W. Nuss is gratefully acknowledged.

References

[1]Reynolds, B. and Lakshminarayana, B., "Characteristics of the Near Wake of a Compressor or a Fan Rotor Blade," *AIAA Journal,* Vol. 17, Sept. 1979, pp. 959-967.

[2]Ravindranath, A., "Mean Velocity and Decay Characteristics of the Near and Far Wake of a Compressor Rotor," *Journal of Engineering for Power,* Vol. 102, July 1980, pp. 535-548.

[3]Reynolds, B. and Lakshminarayana, B., "Characteristics of Lightly Loaded Fan Rotor Blade Wakes," NASA CR 3188, Oct. 1979.

[4]Pierzga, M. J., "Experimental Verification of the Streamline Curvature Numerical Analysis Method Applied to the Flow through an Axial Flow Fan," M. S. Thesis, Dept. of Aerospace Engineering, The Pennsylvania State University, University Park, Pa., 1981.

[5]Lakshminarayana, B., "Techniques for Aerodynamic and Turbulence Measurements in Turbomachinery Rotors," *Journal of Engineering for Power,* Vol. 103, April 1981, pp. 374-392.

[6]Schulze, W. M., Erwin, J. R. and Ashby, G. C., "NACA 65 Series Compressor Rotor Performance with Varying Annulus Area Ratio, Solidity, Blade Angle, and Reynolds Number and Comparison with Cascade Experiments," NACA TN 4130, Oct. 1957.

[7]Lakshminarayana, B. and Reynolds, B., "Turbulence Characteristics in the Near Wake of a Compressor Rotor Blade," *AIAA Journal,* Vol. 18, Nov. 1980, pp. 1354-1362.

[8]Gallus, H. E., Lambertz, J., and Wallmann, Th., "Blade Row Interaction in an Axial Flow Compressor Stage," *Journal of Engineering for Power,* Vol. 102, Jan. 1980, pp. 169-177.

[9]Lakshminarayana, B., Govindan, T. R., and Reynolds, B., "Effects of Rotation and Blade Incidence on the Properties of Turbomachinery Rotor Wake," AIAA Paper 81-0054, Jan. 1981.

[10]Anand, A. and Lakshminarayana, B., "An Experimental Study of Three Dimensional Turbulent Boundary Layer and Turbulence Characteristics inside a Turbomachinery Passage," *Journal of Engineering for Power,* Vol. 100, Oct. 1978, pp. 676-690.